Influence of stress on the photocatalytic properties of sprayed ZnO thin films

Houda Ennaceri, Mourad Boujnah, Darja Erfurt, Jörg Rappich, Xi Lifei, Asmae Khaldoun, Abdelilah Benyoussef, Ahmed Ennaoui, Abdelhafed Taleb

Influence of Stress on the Photocatalytic Properties of Sprayed ZnO Thin Films

Houda Ennaceri [1,2]*, Mourad Boujnah[1], Darja Erfurt[3], Jörg Rappich[4], Xi Lifei[5], Asmae Khaldoun[2], Abdelilah Benyoussef[1], Ahmed Ennaoui[6], Abdelhafed Taleb[7,8]*

[1]Laboratory of Magnetism and Physics of High Energies, Mohammed V University, Morocco
[2] School of Science and Engineering, Al Akhawayn University, Ifrane 53000, Morocco
[3] PVcomB, Helmholtz Zentrum Berlin für Materialien und Energie GmbH, Schwarzschildstr. 3, 12489 Berlin, Germany
[4] Helmholtz-Zentrum Berlin für Materialien und Energie GmbH, Institut für Si-Photovoltaik, Kekuléstr. 5, 12489 Berlin, Germany
[5] Young Investigator Group Oxygen Evolution Mechanism Engineering, Helmholtz-Zentrum Berlin für Materialien und Energie GmbH, 12489 Berlin, Germany
[6] Institut de Recherche en Energie Solaire et Energies Nouvelles (IRESEN), Morocco
[7] PSL Research University, Chimie ParisTech - CNRS, Institut de Recherche de Chimie Paris, Paris, 75005, France
[8]Sorbonne université, Paris, 75231, France.

*Corresponding Authors: h.ennaceri@aui.ma, abdelhafed.taleb@upmc.fr

Abstract

Zinc oxide (ZnO) thin films grown on glass substrates are prepared by means of the Ion Layer Gas Reaction process. The XRD pattern revealed that the ZnO lattice parameters decrease continuously, with the increasing of the film thickness, indicating a continuous variation in the compressive strain. The influence of the thickness on the optical, morphological and structural properties of deposited ZnO thin films was investigated. The UV-Vis absorption spectra of deposited thin films were shown to exhibit a blue-shift, resulting in an increase in the optical band gap from 3.13 eV to 3.24 eV. Structural parameters such as crystallite size, lattice parameters, Zn-O bond length, and residual stress have been determined, and the compressive strain (tensile stress) is found to increase with the increasing of spray time and in turn deposited thin film thickness. The PL spectra of deposited ZnO films, show stronger PL intensity with increasing deposited thin film thickness, which confirm the influence of deposited film thickness on the recombination process of charge carriers and thus on its optical properties. These results, were confirmed by the photo-electrochemical experiments. In addition, a wettability alteration

and shift from hydrophobic to hydrophilic surface is observed under UV light exposure, which shows that structural defects and surface morphology of deposited thin films were also demonstrated to have a direct impact on deposited films' optical properties. Furthermore, to further confirm these experimental optical results, theoretical first principle calculations were conducted. In addition, a wettability alteration and shift from hydrophobic to hydrophilic surface is observed under UV light exposure.

Key Words. ZnO, Ultrasolic Spray Pyrolysis, Density Functional Theory, compressive strain, photoelectrochemical performance.

1. Introduction

This last century photovoltaic and photocatalytic approaches appear to be serious alternatives to replace fossil fuels, which is responsible for most of the environmental pollution. These approaches allow respectively the conversion of sunlight energy into electrical and chemical energy (green energy). This energy transition is becoming credible, meanly due to tremendous progress and development in material science. Different metal oxides such as TiO_2, ZnO, In_2O_3, SnO_2 and Nb_2O_5 have been used as photo-anodes to convert sunlight energy into green energy. Among them ZnO is considered as one of the most studied semiconductors because of its various properties such as, conductivity change under illumination, high transparency in the visible spectral region [1] and photocatalytic capability [2]. Furthermore, ZnO is basically hydrophilic [3, 4], nevertheless, hydrophobic surfaces can be prepared by creating dual-scale rough structures [5]. ZnO crystallizes on three main forms: the hexagonal wurtzite, the cubic zinc blende, and the cubic rocksalt. The hexagonal wurtzite crystal structure (space group C6V = $P6_3mc$) is known to be the most stable and the most common phase of ZnO. The zinc blende is a metastable structure (space group$F\bar{4}3m$), which can only be stabilized by heteroepitaxial growth on cubic substrates. High pressure induces a transition from the wurtzite structure to the rocksalt structure (space group$Fm3m$) at around 10 GPa [6].

Due to its properties, ZnO is a potential material candidate for various applications including, gas sensors [7], anti-reflective-coatings [8], LED [9], dye sensitized solar cells [10] and UV photo catalysis [11]. Different applications share the same required properties such as high specific surface, absorption band extension to visible and infrared spectral region. For photovoltaic and

photocatalytic water splitting application, the same mentioned properties are required and ZnO is considered to have a promising potential as photo-anode for these applications. For water splitting, photo catalytic process induces the production of hydrogen and oxygen within the NIR, Visible and UV spectral range. Due to the recombination process of excitons and the limited light absorption of semiconductors material, the sunlight energy conversion is low. To improve this conversion efficiency, the deep understanding of different semiconductor properties is needed.

To prepare ZnO thin films, different preparation techniques have been developed such as sol gel [12], RF magnetron sputtering [13], chemical vapor deposition [14], ink-jet printing [15], electrochemical deposition [16] and spray pyrolysis [17]. Among them, the spray pyrolysis technique has several advantages, such as simplicity and low cost, control of the films' chemical uniformity and homogeneity, and the scaling-up possibility to produce large surface thin films.

Depending on the ZnO preparation method and conditions, powder or thin film could be obtained. Although ZnO powders have higher photocatalytic performance compared to thin films, the major advantage of using ZnO thin films in photo-catalytic applications rather than ZnO powders is the better recovery for reusability. In fact, for ZnO thin films, the catalysts and reaction products do not have to be separated, as it is the case for ZnO powders or colloidal suspensions [18]. Moreover, using ZnO in thin films form can prevent or decrease light scattering, which increases the transmittance of light, and would result in an enhanced photo-catalytic activity [19]. However, thin films photo-catalysts generally have lower surface areas compared to powders, leading to surface area constraints, and inferior intrinsic photocatalytic performance in comparison to powders [20, 21]. The foremost impact of surface morphology, crystal structure, compactness and surface defects on the photocatalytic and photovoltaic performance of semiconductors is largely discussed in the literature [22]. In fact, thin films exhibiting smaller grain size are reported to have higher surface area, which facilitates and increases the interaction between the photo catalyst's surface and the adsorbed species or sunlight [23].

Many work in the literature established the effect of UV light exposure on the wettability and therefore the photocatalytic activity of ZnO. It has been reported that hydrophilic property of ZnO coated surfaces containing photo-catalytic particles can be triggered by the ultraviolet

irradiation. Upon exposure to UV light, electron/hole pairs (e^-/h^+) are generated in the surface of ZnO thin films, which results in a switching in the wetting behavior from hydrophobic to hydrophilic according to the following process [24]:

$$ZnO + 2\hbar v \rightarrow 2h^+ + 2e^- \quad (1)$$

$$O^{2-} + h^+ \rightarrow O^{1-} \text{ (Surface trapped hole)} \quad (2)$$

$$Zn^{2+} + e^- \rightarrow Zn_s^+ \text{ (Surface trapped electron)} \quad (3)$$

$$O^{1-} + h^+ \rightarrow \tfrac{1}{2} O_2 + V_o \text{ (Oxygen vacancy)} \quad (4)$$

The reaction of photo generated holes with lattice oxygen (Eq. 2) results in the formation of oxygen vacancies, and the reaction of electrons with lattice Zinc ion leads to the formation of defective (Zn_s^+) sites (Eq. 3). The presence of oxygen vacancies at the surface of ZnO films increases the water adsorption at the film's surface when irradiated with UV light, making the surface more hydrophilic. The photo catalytic performance of thin films is deeply affected by several factors such as the crystal structure, surface area, crystallite size, chemical composition and surface defects and film thickness [25, 26]. All these factors are entangled and their effects on the photocatalytic performance of the films are difficult to untangle for immobilized thin films. They are also very sensitive to the deposition technique and the deposition parameters. Recent work by Ramirez-Canon et al. [27] show that the parameters that affect photocatalytic activity of immobilized photo catalysts are light absorbance capacity and crystal size, rather than surface area. Despite the fact that the photo catalytic reaction is fundamentally a surface reaction, the dependence of the photo catalytic activity on the film thickness has been observed and reported for different materials such as titanium dioxide [28], indium tin oxide [29], hematite [30], and zinc oxide [31]. In most cases, the photo catalytic performance is shown to strongly depend on the film thickness.

In this work, transparent wurtzite ZnO thin films with nano-petal structures are prepared by the Ion Layer Gas Reaction technique. The effect of thickness and spray time on the optical, structural and morphological properties is investigated. Also, the photocatalytic activity is assessed by photoluminescence measurements as well as photo-electrochemical testing. This work attempts to correlate the photocatalytic activity with the surface morphology, crystallinity,

structure and defects of the ZnO thin films, which are very important parameters to assess the performance of ZnO electrodes for photovoltaic and water splitting applications.

2. Experimental

2.1. Materials and Methods

The ZnO thin films were deposited by the Spray-ILGAR technique, following the procedure explained in our previous work [32]. Low iron soda lime glass (provided by Berliner Glas KGaA Herbert Kubatz GmbH & Co) was used as substrate. The precursor solution with 20 mM concentration was prepared by dissolving ($C_{10}H_{14}O_4Zn.H_2O$) in pure Ethanol using an ultrasonic device. Prior to the deposition, the glass substrates heated to a temperature of 400°C and the deposition was performed using Nitrogen as a carrier gas, with a flow rate of 5 liters per minute, and a spraying rate of 25 ml per 15 minutes.

2.2. Thin Film Characterization

The structural characterization and chemical composition of deposited thin films was achieved by X-ray diffraction using a Siemens D5000 diffractometer. The phase and crystal structure were identified using Cu-Kα radiation source with λ= 1.5406Å and a secondary monochromator in the range 2θ from 20° to 80° (cathode voltage: 40 kV, current: 40 mA).

The surface morphology of deposited thin film was examined by means of scanning electron microscopy on a Zeiss Ultra 55 microscope (acceleration voltage: 10 kV) and the atomic force microscopy (AFM) measurements were performed using a XE-70 SPM with a silicon tip (PPP-NCHR). The film thickness was also confirmed using SEM cross sections. The spectroscopic analysis (UV-VIS transmission and absorption spectra) was achieved using a Perkin Elmer Lambda 950 spectrophotometer. The photoluminescence measurements were conducted in a system consisting of a pulsed dye laser pumped by a nitrogen laser from Lasertechnik Berlin, with a prism monochromator from Zeiss, and a Si-photodiode detector which is time integrating over about 200mue sec.

The photo-electrochemical (PEC) measurements were accomplished in a Teflon cell equipped with a quartz window. Ag/AgCl and platinum were used as a reference and a counter electrodes, respectively. The photocurrents were conducted using an AM1.5 solar illumination (100mWcm^{-}

^{2}) with a WACOM super solar simulator (WXS-50S-5H, class AAA). A 0.1 MKPi buffer solution (pH=7) was used as electrolyte for PEC measurements. 2.0M potassium nitrate (KNO_3) was added to the electrolyte solution.

The surface chemical composition was investigated by X-ray photoelectron spectroscopy (XPS) using a MAC II RIBER photo-electron analyzer with an Mg-Kα radiation source (hυ = 1256.6 eV). The XPS measurements were performed by assessing the intensities of integrated photo peaks after implementing a Shirley background subtraction. The wettability measurements were performed using an OCA 15 plus goniometer. The wetting properties under UV irradiation were investigated using a 1400 W Xenon lamp from Müller Elektronik-Optik.

The photocatalytic activity of the films is assessed by measuring the degradation of the methylene blue (MB) under UV irradiation. The ZnO films (1.5x2.5cm^2) were placed in a 6-well plate (Thermo Fisher Scientific, Nunclon Delta Surface), and immersed in 4 mL of a 5 µmol/L MB aqueous solution. The plate was positioned under a Heraeus Original Hanau Suncare tanning tube UVA-lamp with a radiant flux density of 7.6 mW cm^{-2} (OH N21/25 Slim). During the UV illumination, the plate was constantly shaken on a Titramax 100 (Heidolph Instruments GmbH & Co. KG) with a rotation speed of 200 rpm. The dye absorption was periodically measured at 660 nm using a Tecan Reader infinite M200 spectrometer, and the degradation of methylene blue was calculated accordingly.

3. Results and Discussion

3.1. Structural Properties

ZnO thin films with different thicknesses were deposited, by varying the deposition time, the spray times were fixed as 30 min, 45 min, 1 hour and 2 hours, achieving thin film thicknesses of 100 nm, 230 nm, 305 nm, and 720 nm, respectively. As it can be observed from Fig. 1 ZnO thin film thickness versus deposition time show a quasi-linear behavior.

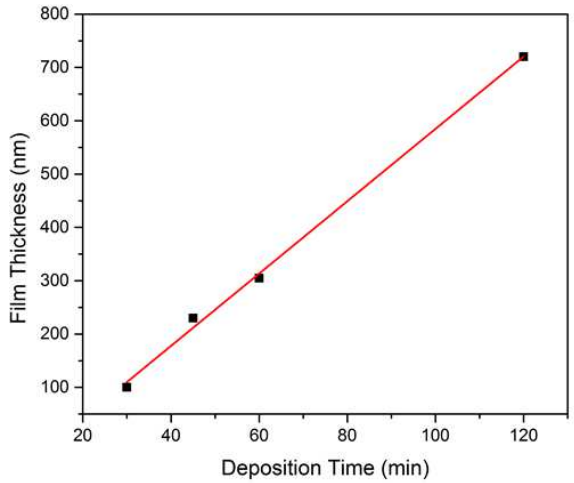

Figure 1. Variation of the film Thickness with the deposition time.

The XRD analysis (Fig. 2) shows the presence of the ZnO wurtzite phase according to the powder diffraction card of ZnO (JCPDS 36-1451). All deposited thin films with different thicknesses are oriented along (002) crystallographic plane, and the growth takes place along the c-axis direction, which is explained by the fact that the ZnO (0001) crystallographic plane is characterized by a thermal stability as well as a lower surface energy. It is shown from the XRD pattern (Fig.2) that the increase of the ZnO thin film thickness results in more intense and narrower diffraction peaks. The full width at half maximum (FWHM) decreases with increasing thickness, indicating larger grain size and better crystallinity of deposited thin films.

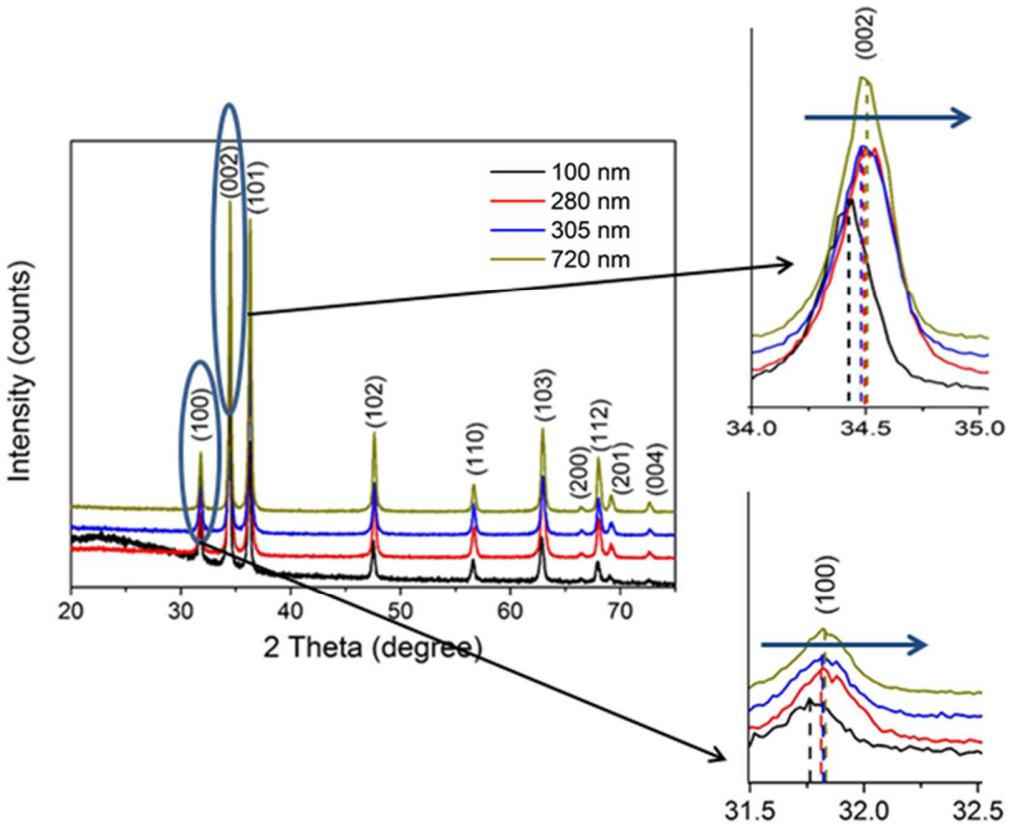

Figure 2. XRD pattern of ZnO thin films prepared with different spray times.

Close inspection of the XRD spectra reveals that all the XRD peaks shift towards higher angle with increasing thickness of ZnO, which indicates the occurrence of residual stress in the thin films. The shifting towards higher angles indicates that the thin films are under compressive strain [33].

Table 1. Comparison between the 2 θ values for the (002) plane with the standard value for ZnO value.

	2 θ values for the (002) plane	
Sample	**Observed**	**Standard [34]**
100 nm	34.443°	34.40°
230 nm	34.463°	34.40°
305 nm	34.501°	34.40°
720 nm	34.516°	34.40°

The 2θ values for the (002) crystallographic plane of all deposited ZnO thin films are larger compared to the bulk ZnO (2θ = 34.40°) [34], which implies that the prepared thin films are exposed to compressive strain in the c-axis direction. Higher shifting in the diffraction angles is observed for thicker ZnO thin films compared to the standard reference value, which indicates higher compressive strain in the sample corresponding to the thickness of about 720nm.

The grain size can be estimated from the FWHM of the high intense peaks, namely the one corresponding to (002) crystallographic plane, using the Scherrer formula [35, 36]:

$$D = \frac{K\lambda}{\beta_D \cos\theta} \tag{5}$$

Where D is the grain size, the constant K is the shape factor (K = 0.9), λ is the wavelength ($\lambda = 1.54$ Å), β_D is the line broadening at half-maximum intensity (FWHM), and θ is the Bragg diffraction angle. It can be observed from Table 2 that the average crystallite size steadily increases with increasing thin film thickness, which is attributed to the fact that thicker thin films undergo longer heat treatment. The lattice constants for the ZnO hexagonal structure have been calculated using Bragg's law [37]:

$$2d_{hkl} \sin\theta = n\lambda \tag{6}$$

Where (d_{hkl}) is the inter-planar spacing given in Eq. (3) [38, 39], θ is the Bragg diffraction angle, n is the diffraction order (n = 1), and λ is the $Cu\ K\alpha$ radiation wavelength (λ = 1.54 Å)

$$d_{hkl} = \frac{1}{\sqrt{\frac{4}{3}\left(\frac{h^2 + k^2 + hk}{a^2}\right) + \frac{l^2}{c^2}}} \tag{7}$$

The a-lattice constant of the ZnO thin films are estimated from the XRD peak corresponding to (100) crystallographic plane using the following equation [40]:

$$a = \frac{\lambda}{2\sin\theta_{(100)}} \sqrt{\frac{4}{3}(h^2 + hl + k^2) + \left(\frac{a}{c}\right)^2 l^2} \tag{8}$$

$$a = \frac{\lambda}{\sqrt{3}\sin\theta_{(100)}} \tag{9}$$

The c-lattice constant of the ZnO thin films are estimated from the XRD peak corresponding to (002) crystallographic plane using the following equation:

$$c = \frac{\lambda}{2\sin\theta_{(002)}}\sqrt{\frac{4}{3}\left(\frac{c}{a}\right)^2(h^2 + hl + k^2) + l^2} \tag{10}$$

$$c = \frac{\lambda}{\sin\theta_{(002)}} \tag{11}$$

The lattice constants of the bulk ZnO are (a = b = 3.2498 Å) and (c = 5.2066 Å) [41]. The calculated lattice constants of the ZnO thin films with different thicknesses are presented in Table 2.

In order to identify the nature of strain along the c-axis perpendicular to the film's substrate surface, a comparison between these deposited ZnO thin films and the lattice constant of the bulk ZnO (c = 5.2066 Å) is conducted. ZnO thin films exhibiting lower values compared to the bulk are subject to compressive strain along the c-axis, while thin films exhibiting higher values compared to the ZnO bulk are subject to tensile strain along the c-axis. In the present work, all deposited ZnO thin films exhibited lattice c values lower than that of the bulk ZnO, which implies that the ZnO thin films with different thicknesses are under the state of compressive strain along the c-axis perpendicular to the substrate surface, which implies a unit cell compression along the c-axis direction. Moreover, from the values presented in Table 2, it can be observed that the lattice parameters a and c decrease with increasing thin film thickness. Malek et al. expalined this phenomenon by the presence of dangling bonds, possessing unpaired electrons, and forming electric dipoles [42]. This will lead to the increase in the electrostatic attraction between the zinc and oxygen ions (Zn^{2+} and O^{2-}) ions, and hence resulting in lattice compression. From the XRD patterns (Fig. 2), it can be observed also that the peaks are shifting towards higher angles compared to the bulk as the thin film thickness increases, indicating the presence of compressive strain. The unit cell volume of hexagonal structure of ZnO thin films is calculated from its lattice constants using Eq. 12:

$$V = \frac{\sqrt{3}}{2}a^2c \tag{12}$$

The unit cell volume values of different prepared samples are presented in Table 3. It is apparent that the unit cell volume decreases with increasing thin film thickness and that the smallest unit cell volume is observed for the highest deposited thin film thickness of 720 nm. The decrease in the unit cell volume is a consequence of higher residual stress, which is enhanced with thin film thickness. The density of the deposited thin films is also computed using Eq. 13:

$$\rho = \frac{1.6609 \times M \times n}{a^2 c \sqrt{\frac{3}{4}}} \tag{13}$$

Where ρ is the density of different prepared thin films, M is the molecular weight of ZnO (M=81.408 g/mol for ZnO), and n is the number of molecules per unit cell (n=2), a and c are the lattice parameters of ZnO. The estimated density values are presented in Table 2, and show that the thin film density increases with the increasing of its thickness. This result is in line with the scanning electron microscopy analysis presented in Fig. 3. Additionally, the Zn-O bond length in the c-direction is also calculated from the lattice constants using the following equation:

$$L = \left(\left(\frac{1}{3}\right)\left(\frac{a^2}{c^2}\right) + \frac{1}{4}\right)c \tag{14}$$

As shown in Table 3, a decrease in the Zn-O bond length in the c-direction is observed, with the increase in thin film thickness, which is in agreement with the previous results.

Table 2. Lattice constants, density, and crystallite size of ZnO thin films deposited with different spray times.

	Lattice constant a=b(Å)		**Lattice constant c(Å)**		**Density (g/cm³)**		**c/a Ratio**	**Crystallite Size (nm)**
Sample	**Calculated**	**Standard**	**Calculated**	**Standart**	**Calculated**	**Standard**		
100nm	3.2480	3.2498	5.2015	5.2066	5.6883	5.675	1.6014	24.86
230nm	3.2432		5.1985		5.7083		1.6028	25.73
305nm	3.2431		5.1930		5.7150		1.6012	26.11
720nm	3.2425		5.1902		5.72		1.6	27.04

Table 3. Unit cell volume, Zn-O bond length, stress and strain of the ZnO thin films deposited with different spray times

	Unit cell Volume V(Å^3)		Bond length (Å)	Stress (GPA)	Strain of c-axis (%)
	Calculated	Standard			
100nm	47.5239	47.62	1.9765	0.22	-0.10%
230nm	47.3565		1.9741	0.36	-0.15%
305nm	47.3014		1.9733	0.61	-0.26%
720nm	47.2598		1.9728	0.70	-0.32%

For all deposited ZnO thin films, the calculated values of the lattice constant c are smaller than the value of the bulk ZnO. Therefore, the films are subject to compressive strain and unit cell compression along the c-axis direction, as shown from the lattice constant and strain values (Table 2 and Fig. 2). More evidence that all ZnO deposited thin films are under compressive strain in the c-direction is shown in Table 1. It can be seen also that the diffraction angles of (002) crystallographic plane for all deposited thin films are larger than that of the bulk ZnO. The impact of unit cell compression in the c-axis direction results in a tension force acting in the plane of the deposited thin film, and therefore, an increasing of tensile stress in the lateral direction is generated in deposited thin films. This can be explained by the fact that with the increasing deposition time, the adsorbing atoms have more energy to assemble to the lowest energy levels, and the atomic mobility increases to reduce the structural defects. Therefore, the grains grow bigger, and the density of the films increases (Fig. 3). This results are consistent with the crystallinity improving when deposited thin films thickness increases.

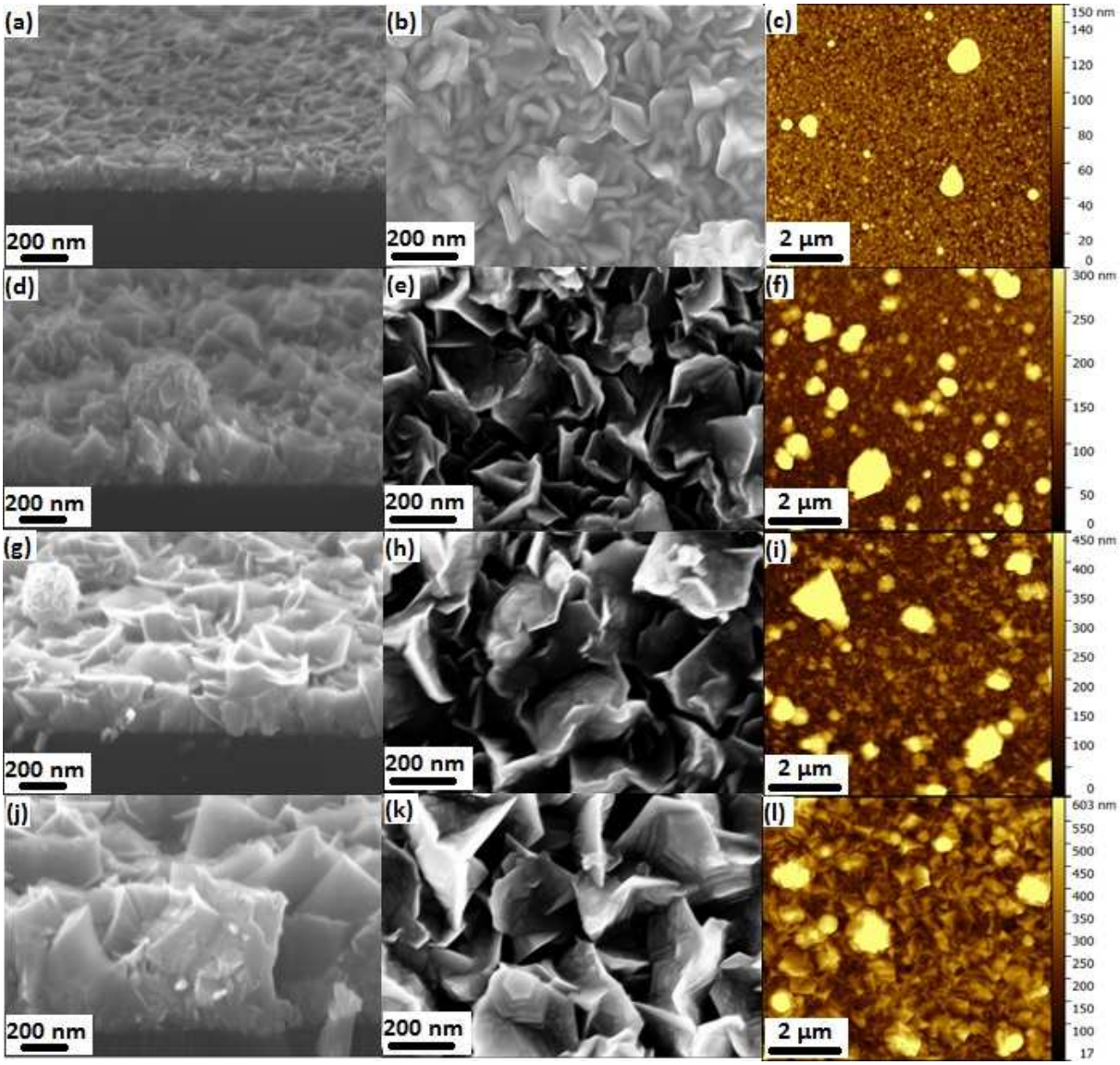

Figure 3. SEM cross section and surface micrographs, and AFM images of deposited ZnO thin films with different thicknesses (a-c) 100nm, (d-f) 230nm, (g-i) 305nm and (j-l)720nm.

The morphology of deposited ZnO thin films was studied by using filed emission gun scanning electron microscopy (FEGSEM) and the results are depicted in Fig. 3. It can be observed that the morphology of deposited ZnO thin films is flower like and cover the whole substrate. Futhermore, ZnO deposited thin films cross section shows dense films with no distinguished porosity. In addition, deposited ZnO thin films keep the same morphology with the sheet section increasing faster than its thickness versus the deposition time, which is a signature of different steps of the same growth mechanism. From the XRD characterisation, it can be observed that the

intense peaks correpond to the (100), (002) and (101) crystallographic planes, which could be assigned to the sheet surface of ZnO. However, closer analysis of the FEGSEM shows that most of the ZnO sheets are more or less perpendicular to the substrate (Fig.3(e), (f), (g) and (h)). In addition, these XRD and FEGSEM results indicate that ZnO deposited thin films is of polycrystalline Wurtzite structure with random growth orientations. This later ZnO thin film characteristic could be attributed to the amorphous nature of used glass substrates for deposition. The AFM investigations allowed the determination of the root mean square (RMS) roughness as 64nm, 118nm and 143nm, for film thickness of 100nm, 230nm and 305nm respectively. It can observed that the RMS roughness increases with deposited film thickness, whereas, a subsequent decreases of the RMS roughness (127 nm) is observed for highest thickness of 720nm.

Furthermore, it is well known that the substrate temperature has a strong influence on the properties of deposited ZnO thin films, according to large literature dealing with this issue. In fact, the increase of substrate temperature enhances the atomic mobility on the surface, reduces the structural defects, and favors a relaxation of the stress in deposited ZnO thin films. For example, it is reported in the literature that deposited ZnO thin films at a lower substrate temperature shows a strong compressive stress, whereas at a high temperature, the strain quickly relaxes due to the high kinetic energy of growing ZnO [43]. Prasada Rao et al [44] reported that ZnO thin film deposited at substrate temperature of 723 K shows low stress, which they explain by thin film thickness or morphology variation.

The average uniform strain (ε_{zz}) in the lattice along the c-axis perpendicular to the substrate surface is estimated from the lattice parameters using the following:

$$\varepsilon_{zz} = \frac{c - c_0}{c_0} \times 100\ (\%) \tag{15}$$

Where c denotes the lattice parameter of the strained hexagonal cell of ZnO thin films, calculated from the (002) XRD peak, and c_0 denotes the unstrained lattice parameter of the bulk ZnO (c_0 = 5.2066 Å [41]. Positive values of the strain (tensile strain) indicate a stretching of the material. On the other hand, negative values of the strain (compressive strain) indicate that the material is being compressed, which is the case for the deposited ZnO films.

The impact of unit cell compression along the c-axis direction results in a tension force acting in the plane of the deposited thin film. Consequently, an increasing tensile stress is generated in deposited ZnO thin films. Therefore, even under compressive strain in the film plane, axial tensile stress is generated by Poisson's effect in the lateral direction (normal to the film plane). The residual stress of the ZnO deposited thin films (ρ_f) is calculated using the following equation:

$$\rho_f = \frac{2C_{13}^2 - C_{33}(C_{11} + C_{12})}{2C_{13}} \times \varepsilon_{zz} \tag{16}$$

Where c_{ij} denote the elastic stiffness constants (c_{11} = 208.8 GPa, c_{12} = 119.7 GPa, c_{13} = 104.2 GPa, c_{33} = 213.8 GPa [45]. Using the indicated values of the elastic stiffness constants, the residual stress is calculated using the following formula:

$$\rho_f = -233 \times \varepsilon_{zz}\ [GPa] \tag{17}$$

Positive values of the stress indicate that the stress is tensile, whereas negative values of the stress indicate that the stress is compressive [46]. The calculated values of strain and stress are indicated in Table 3. It can be observed that the residual stress increases with increasing ZnO deposited thin film thickness (Table 3), which is due to the Zn-O bond length decreasing.

Generally, the total stress in thin films can be either intrinsic or extrinsic stress. The first, being introduced by imperfections during the growth process such as structural defects, distortions in the lattice constants or impurities, and the second being introduced by the difference in the thermal expansion coefficient between the ZnO films and the glass substrate. The linear thermal expansion coefficients of ZnO ($\alpha_{11} = 6.05 \times 10^{-6}\ °C^{-1}, \alpha_{33} = 3.53 \times 10^{-6}\ °C^{-1}$) and soda lime glass ($\alpha_{33} = 9 \times 10^{-6} °C^{-1}$) [47]. The linear thermal expansion coefficient of ZnO is less than that of the glass substrate; therefore, a compressive in-plane stress is exerted by the substrate on the ZnO thin film as it cools down from the deposition temperature of 400 $°C$ to room temperature. The intrinsic stress in the ZnO thin films with different thicknesses is tensile, and its magnitude is higher compared to the compressive thermal component. Moreover, the thermal strain resulting from the difference in the linear thermal expansion coefficient of the

ZnO deposited thin films and the glass substrate is much smaller compared to the measured strain [48], showing that the stress in the thin films originates form the growth process rather than from thermal expansion. Hence, the stress in the films is intrinsic. Additionally, as it has been reported in the literature, extrinsic stress relaxes with increasing film thickness [48]. In the present study, and since the ZnO deposited thin film thicknesses range from 100 nm to 720 nm, the extrinsic stress is ignored and the total estimated stress is predominantly intrinsic.

In the present work, the intrinsic strain of all the prepared samples is compressive in nature. As shown in Table 3, the strain increases with deposited ZnO thin films thickness. As a consequence, thicker ZnO thin film has the highest stress, implying that the degree of crystal imperfections is increases with deposited thin film thickness. It can also be noted that the increase of thin film thickness enhances its crystallite size and increases the residual compressive strain. Furthermore, the positive tensile stress in deposited thin films results from the stretching crystal size, indicating a decreasing lattice constant compared to the bulk ZnO. The tensile stress values increase from 0.22 GPA to 0.70 GPA, when the thin film thickness moves from 100 nm to 720 nm respectively (Table 3).

3.2. Optical Properties

The optical transmittance of deposited ZnO thin films decreases with increasing film thickness as shown in Fig. 4.

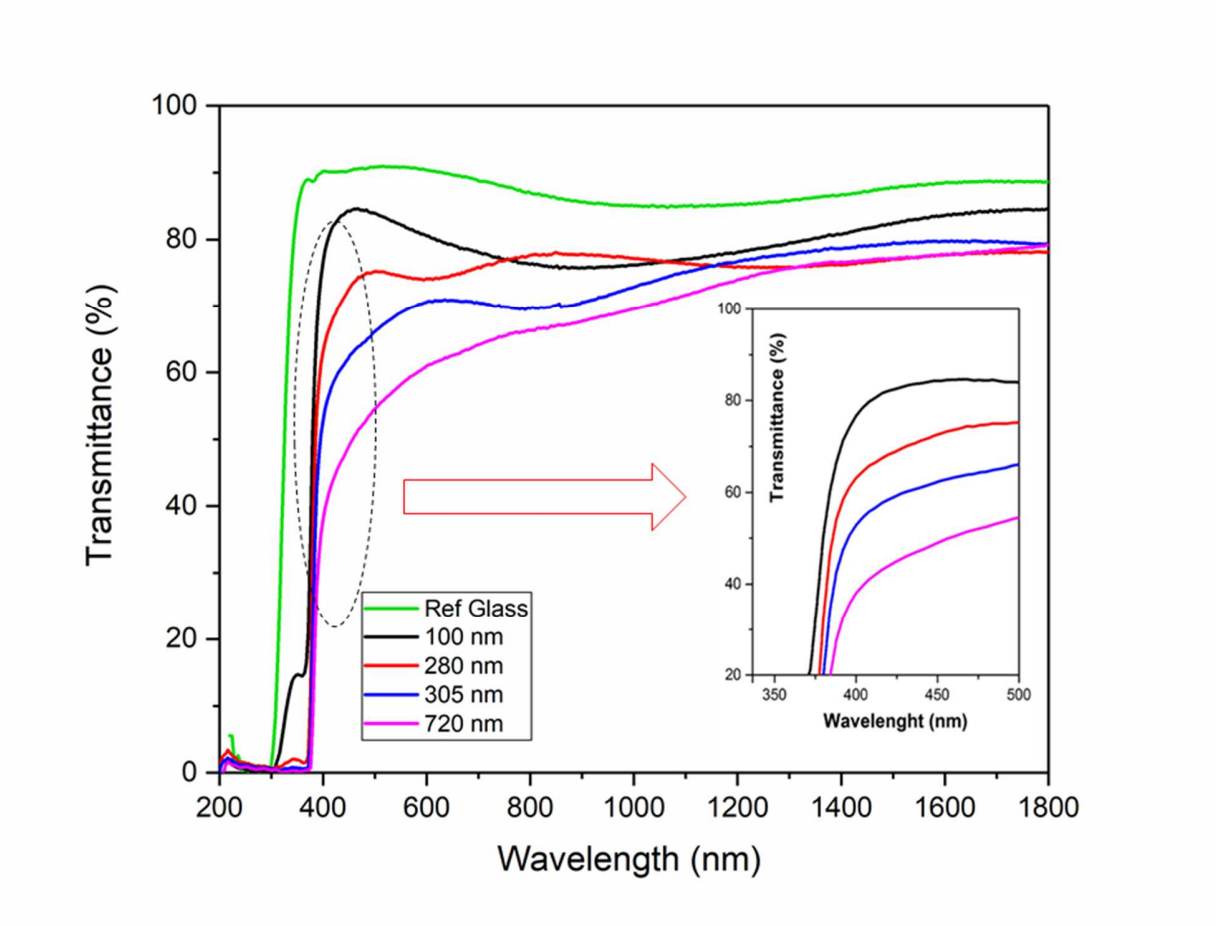

Figure 4. Optical Transmittance Spectra of the ZnO thin films with different thicknesses. The blue shift can be observed from the inset image.

Fig. 4 shows the optical transmittance and Fig. 5(a) the optical absorption (A=1-T-R) spectra of deposited ZnO thin films with different thicknesses of 100 nm, 230 nm, 305 nm and 720 nm (from left to right). It can be observed that all deposited thin films are highly absorbing at wavelength higher than 370 nm, which is the UV cut-off for ZnO absorption.

The optical band gap of the different deposited thin films was calculated by plotting the graph of the incident photon energy (hv) versus $(\alpha hv)^2$, where α is the absorption coefficient that can be spectroscopically calculated from the measured optical transmittance using Eq. 18, where d is the thin film thickness and T is the optical transmission.

$$\alpha = \frac{1}{d}\ln\frac{1}{T} \tag{18}$$

The absorption coefficient is related to the optical band gap as follows:

$$(\alpha hv)^2 = k(hv - E_g) \tag{19}$$

The optical band gap is obtained by the extrapolation of the straight dotted lines of Fig 5 (b) to $(\alpha hv)^2 = 0$. The calculated experimental optical band gap is 3.13 eV, 3.18 eV, 3.20 eV, and 3.24 eV for ZnO deposited thin film thicknesses of 100 nm, 230 nm, 305 nm and 720 nm, respectively.

It can also be observed that the optical band gaps of prepared ZnO thin films are lower than that of the bulk ZnO (3.37 eV). However, the blue-shift of the band gap becomes more evident with the increasing deposited thin film thickness, which is due to the improved crystalline structure with the increasing of spray time.

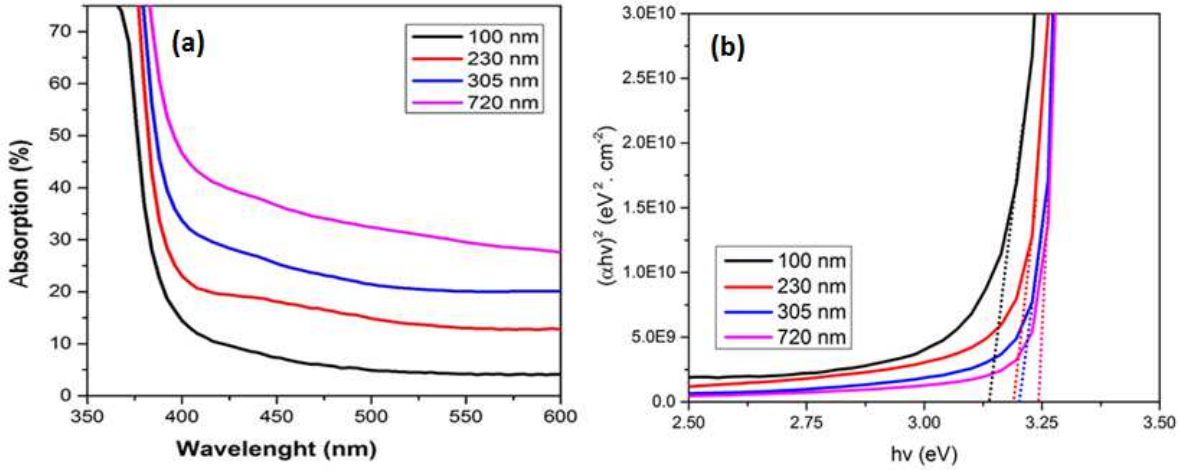

Figure 5. (a) UV-Vis Absorption Specta (b) Direct band gap of deposited ZnO thin films prepared with different spray times.

Because of stress increasing (Table 3), the band gap was found to be increasing with increasing film thickness (as illustrated in Fig. 5). This is due to the decrease in the lattice parameter, which implies that the atoms get closer. It can be observed that the energy band gap increases as the compressive strain/tensile stress increases, which is in good agreement with previous studies that show that the strain affects the inter-atomic spacing of semiconducting materials, and that the band gap increases with compressive strain along the c-direction [49]. When the lattice parameter becomes smaller (compressive strain), atoms get closer, therefore their valence electrons get closer, which increases the electrostatic potential energy (U), and makes it more

difficult for the electrons to move to the conduction band, which consequently increases the band gap.

In order to validate the experimental results, theoretical calculations using the density functional theory (DFT) are conducted in order to investigate the effect of compressive strain on the optical properties of ZnO thin films. The theoretical study was conducted through ab initio first principle calculations within the WIEN2k package [50]. The PBE approximation (Perdew Burke Ernzerhof) [51] was used to calculate the exchange and correlation contributions, and the new modified Becke-Johnson (mBJ) potential [52] was used:

$$\upsilon_{\chi,\sigma}^{mBJ}(r) = c\upsilon_{\chi,\sigma}^{BR}(r) + (3c-2)\frac{1}{\pi}\sqrt{\frac{5}{12}}\sqrt{\frac{2t_\sigma(r)}{n_\sigma(r)}} \tag{20}$$

Where:

- $\upsilon_{\chi,\sigma}^{BR}$: the Becke Roussel (PB) potential
- t_σ : the spin dependent kinetic energy density
- n_σ: the spin dependent electron density
- C: a system dependent parameter

The PB potential was initially suggested to imitate the Slater potential. The system dependent parameter c can be determined according to Tran and Blaha work using the following equation for bulk crystalline materials [52]:

$$c = \alpha + \beta\left(\frac{1}{V_{cell}}\int_{cell}\frac{|\nabla_n(r')|}{n(r')}\,\mathrm{d}^3r'\right)^{1/2} \tag{21}$$

The Monkhorst-Pack division was used to create a set of k-points within the Brillouin zone (l_{max} = 10, $Rmt*K_{max}$ = 7.0). The experimental optical results are compared to the theoretical calculations performed using the mBJ approximation. It can be observed from Fig. 6 that the mBJ approximation corroborates with the experimental results.

In order to compare with first-principle calcuations, we considered four sizes of hexagonal ZnO thickness ranging from 100 nm to 720 nm by using the experimental lattice parameters as indicated above. According to what was proved experimentally (Table 2), we found that the reduction of the lattice parameters comes by increasing the size of the thickness, which points

out that there is a compressive strain on the structure. Taking into consideration the lattice parameters of the bulk ZnO as reference, we apply the compression strain for thicknesses of 100nm, 230 nm, 305 nm, and 720 nm, respectively. Afterward, we relax our structure to find the stable parameters. Then the geometry relaxation of all the considered systems maintain an almost unchanged hexagonal structure.

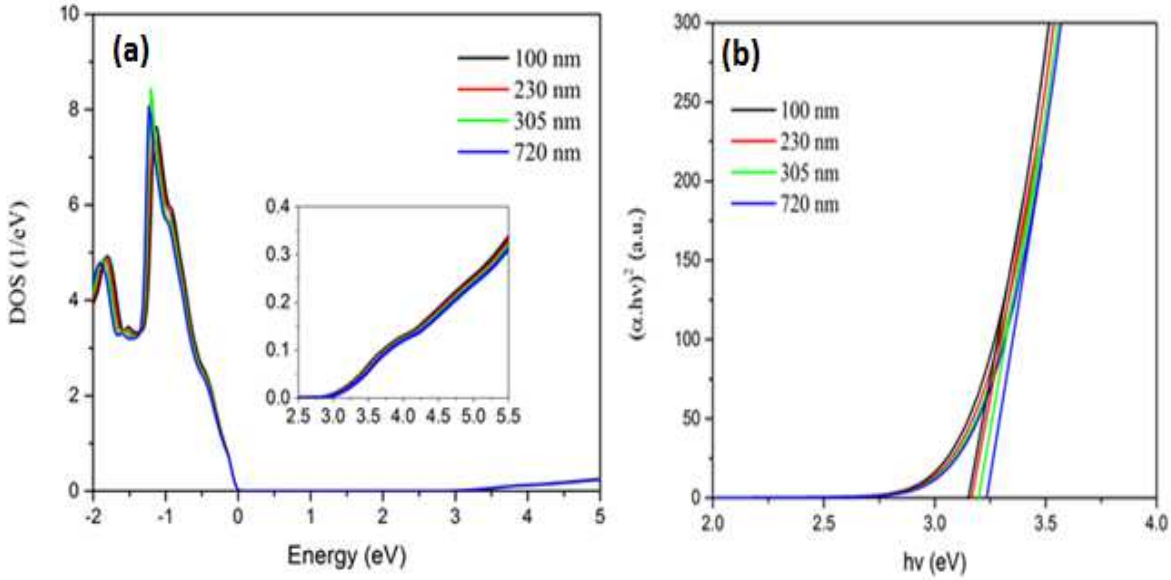

Figure 6. (a) Total density of state of ZnO thin films with different thicknesses (b) Optical band gap of ZnO thin films with different thicknesses using the mBJ approximation

As clearly shown in Fig. 6, the band gap from the total density of state (DOS) increases, when thin films thickness increases from 100 nm to 720 nm under a compressive strain, which is the case if compared to our experiemantal results. To confirm this behavior, we calculate the optical band gap as it is shown in Fig. 6(b) and as it can be clearly observed, the band gap increases with the thickness under a compressive strain, which is in agreement with our experiemantal results. The calculated values of the optical band gap estimated with the simulation are 3.14 eV and 3.24 eV, for thicknesses of 100 nm and 720 nm respectively.

3.3. Chemical Characterization

X-ray photoelectron spectroscopy (XPS) measurements were performed in order to characterize and investigate the chemical state of deposited ZnO thin films with different thicknesses. The XPS spectra were recorded using Mg-Kα radiation (1256.6 eV), and the extended scan is shown in Fig. 7. The XPS spectra corresponding to the Zn 2p shows sharp peaks, indicating the presence of Zn^{2+} lattice ions.

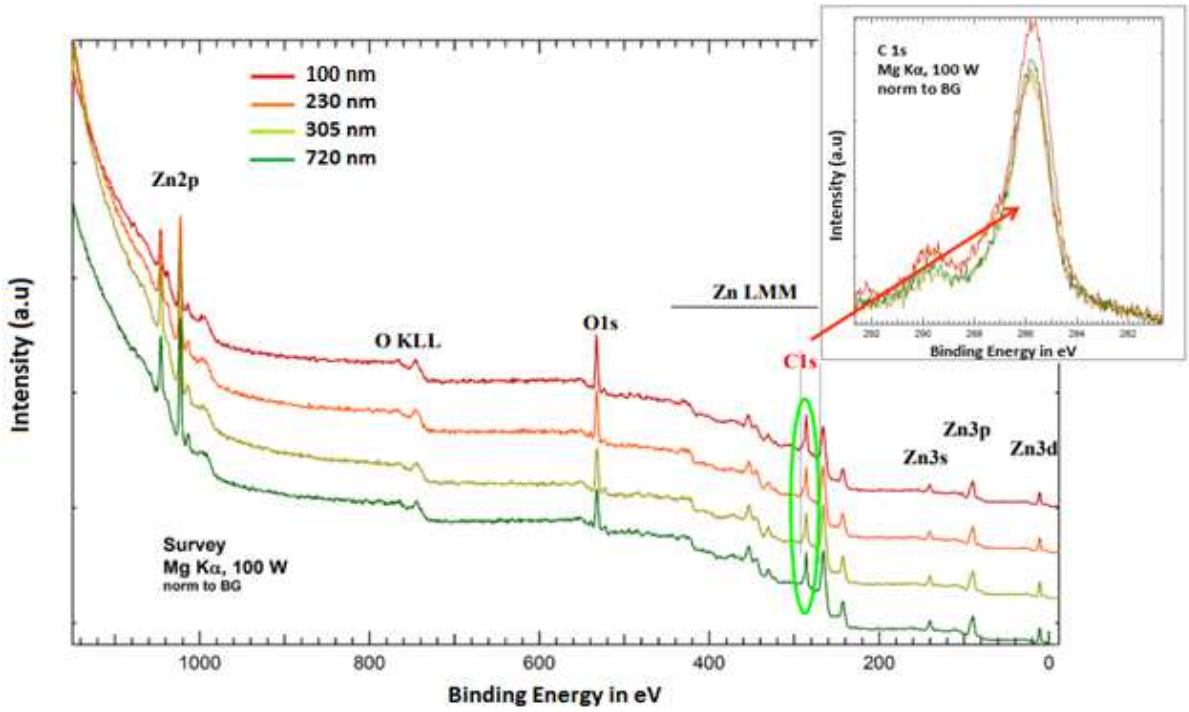

Figure 7. Extended scan of XPS Spectra for the ZnO thin films with different thicknesses.

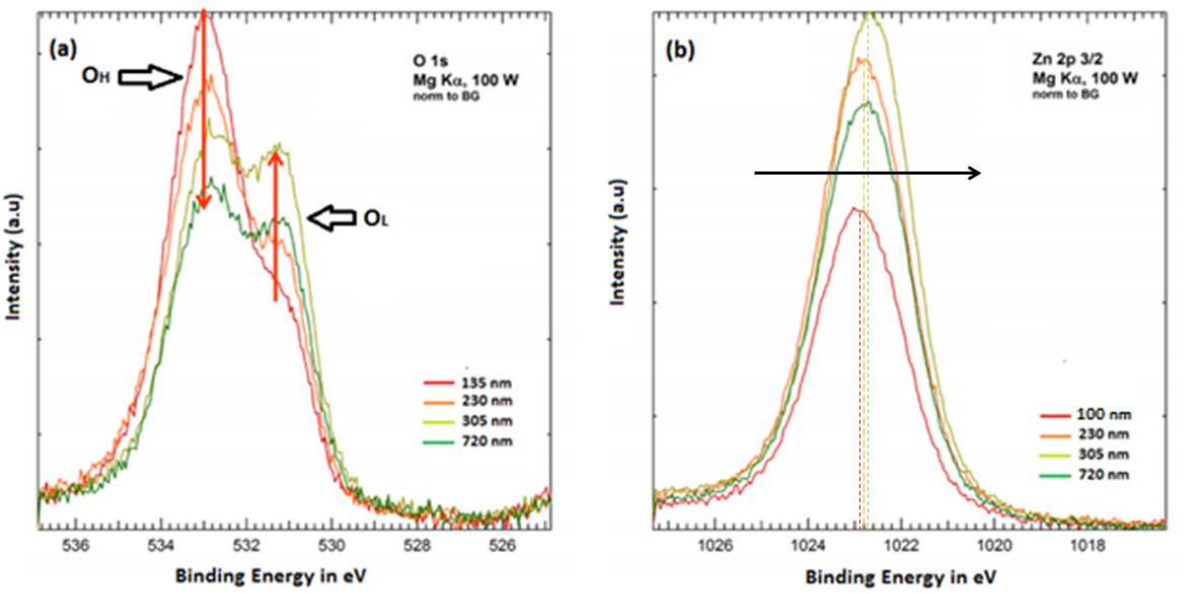

Figure 8. (a) O 1s XPS spectra of ZnO thin films (b) Zn 2p 3/2 XPS spectra of ZnO thin films.

Fig 8 (a) shows the O1s core level spectra, which is resolved in two peaks. The first peak (O_L) centered at binding energy of 531.57 eV is ascribed to lattice oxygen in the ZnO crystal [53]. On the other hand, the second peak (O_H) located at a higher binding energy of 533.25 eV, is attributed to the presence of oxygen vacancies in the ZnO matrix, which is in agreement with XPS results reported in the literature [54]. As represented in Fig. 8 (a), deposited ZnO thin films by the ILGAR technique exhibit a strong dependency between the O/OH^- ratio and the deposition time. By comparing the peak intensities (Fig 8 (a)), it can be observed that, while increasing the deposition time and film thickness, the main lattice oxygen peak (peak O_L) increases whereas the hydroxyl peak (peak O_H) decreases. This means that the quantity of the adsorbed OH^- decreases with increasing film thickness, and can be explained by the reaction of Zn-based precursor on the surface during the deposition procedure. Therefore, the transformation of the Zn-based precursor (zinc hydroxide) to ZnO is dependent on the substrate temperature and the heating time. Hence, for a longer deposition time we have more oxide than hydroxide.

Also, it can be observed form Fig 8 (b) that the Zn 2p 3/2 binding energy is shifting towards lower binding energy as the thickness increases. The binding energy for Zn 1p 3/2 is centered at 1022.9 eV for the lowest thickness of 100 nm (Fig 8 (b)), and is shifted to 1022.7 eV for the 720 nm thick ZnO thin film. These results are in good agreement with the work of Mosquera et al.

[55], showing that a shift of core-level energies to lower binding energies is possible when the grain size increases, and leading to quantum confinement effect.

As checking the stoichiometric formation of deposited ZnO thin films, the Zn/O ratio was determined to be 1.12, 1.16, 1.39, and 1.59 for thicknesses of 100 nm, 230 nm, 305 nm, and 720 nm, respectively. It can be observed that the atomic ratio of Zn to O is higher than 1 for all samples, which suggests the presence of oxygen vacancies at the surface of the prepared samples [56]. Oxygen vacancies act as active sites, and therefore, can easily combine with other reactive species. The atomic ratio of Zn to O increases with the thickness, suggesting an increase in the concentration of oxygen vacancies as the deposition time increases. Also, there is a direct relation between oxygen vacancies and visible light absorption [57], which explains the increase of optical absorption with increasing film thickness.

3.4. Wetting Properties and Photoelechtrochemical Test

The water contact angles measurements show an inverse relation between the contact angle and the surface roughness, with the highest contact angle obtained from the ZnO thin film with the lowest thickness of 100 nm (WCA=98°). The surface morphology and wettability are related according to the Wenzel model and Cassie-Baxter model. The Wenzel model is expressed as follows: where r is the roughness factor, and (θ_r) and (θ) are the apparent contact angles on rough and smooth surfaces, respectively:

$$\cos\theta_r = r\cos\theta \tag{22}$$

On the other hand, the Cassie-Baxter model is expressed as follows:

$$\cos\theta_r = f(\cos\theta - 1) - 1 \tag{23}$$

Where (f) is the Cassie-Baxter roughness factor, which is the fraction of the liquid-solid interface. Both the Wenzel model and the Cassie-Baxter models show that the hydrophobicity increases with surface roughness. However, an inverse relationship between the surface roughness and the contact angle is observed for the ZnO films with different thicknesses. The water contact angles are 98°, 90°, 84°, and 82° for 100 nm, 230 nm, 305 nm, and 720 nm, respectively (Fig. 9).

According to the Cassie-Baxter model, an increase of the surface fraction (f) would lead to a decrease in the water contact angle (θ_r). The roughness can increase if the supporting nano-petals under the water droplet become closer to each other and roughly perpendicular to the substrate. Since in most cases, the superhydrophobic behavior is due to the air trapped within the surface nanostructure, the distance between nanopetals in the present deposited nanostructured must be as small as possible [58]. However, the size and the orientation of nanopetals in deposited ZnO thin film will influence strongly the surface roughness, which can influence in turn the pinning effect of the surface roughness.

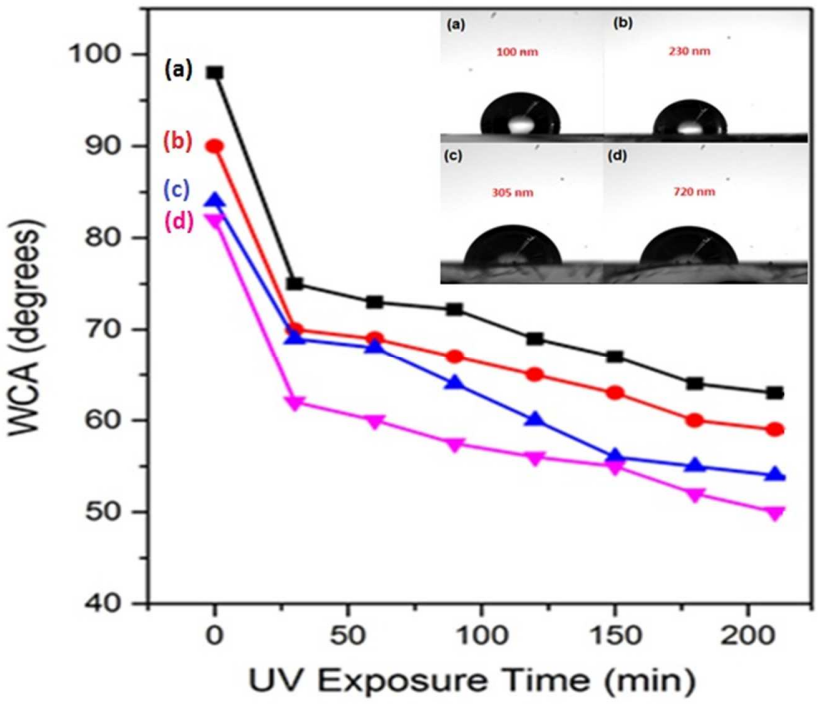

Figure 9. Water contact angle measurements under UV light exposition of different ZnO thin film thicknesses, the inserts are the corresponding contact angle before UV exposure.

The water contact angles of prepared samples were recorded under exposure to UV irradiation for different times ranging from 30 minutes to 210 minutes. The contact angle measurements were taken every 30 minutes time interval. A decrease in the contact angle is observed for all samples and a surface transition between hydrophobic and hydrophilic is perceived. After 3.5 hours of UV exposure, the lowest contact angle is observed for the highest thickness of 720 nm

(Fig. 10). This is explained by the increase in the water adsorption on the film's surface with increasing film thickness.

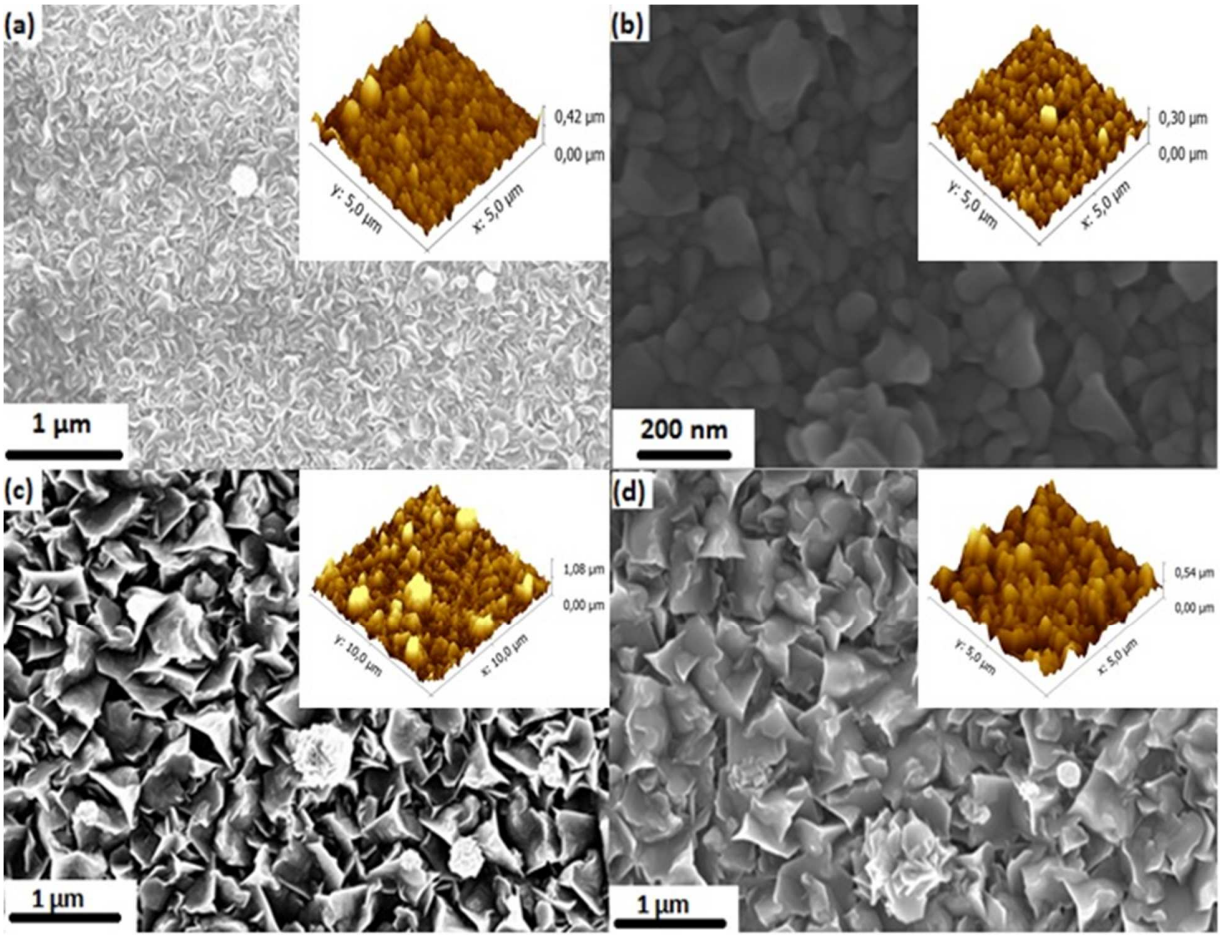

Figure 10.Surface morphology change of different deposited ZnO thin films, (a, b) 100 nm thickness (c, d) 720 nm thickness before (left) and after (right) annealing treatment at temperature of 500°C and over 60min.

In order to investigate the influence of annealing treatment on the surface of deposited ZnO thin films, the roughness and the surface tension were measured before and after the treatment. By using the AFM, the roughness of thinner (100nm) and thicker (720nm) deposited ZnO thin film was measured before and after annealing treatment at temperature of 500°C and over 60 min. The obtained results show that the roughness decreases for both samples. It was observed that the RMS roughness decreases from 64 nm to 30 nm for thinner deposited ZnO thin film (100 nm) and from 127 nm to 69 nm for thicker film (720 nm) (Fig. 10). As a consequence, a water

contact angle was observed to decrease from 98° to 91° and from 82° to 79° for deposited ZnO thin film with thickness of 100 nm and 720 nm respectively. These results are in good agreement with the fact that the heat treatment induces the roughness decreasing and the appearance of surface hydrophilic behavior.

The PL spectra of the sprayed ZnO thin films are depicted on Fig. 11 and the measurements were performed in the range from 370 nm to 800 nm, with 365 nm excitation wavelength. Two main PL emissions are observed: the first peak is a UV-emission peak at 381 nm and the second is a broad green emission peak at 518 nm. The UV emission peak is attributed to free exciting recombination, whereas the broad green emission at 518 nm corresponds to the structural defect, such as oxygen vacancies.

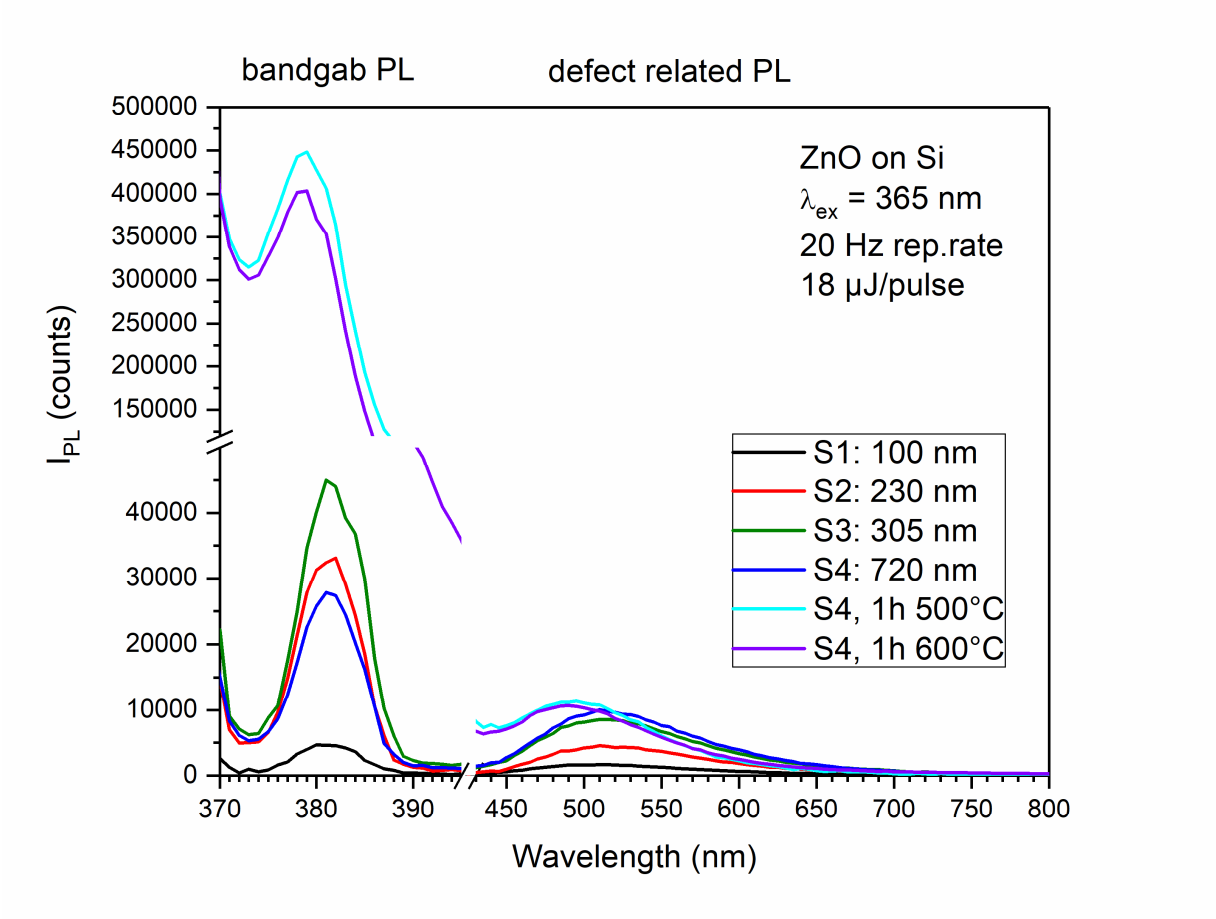

Figure 11. Photoluminescence spectra of sprayed ZnO thin films with different thicknesses

As observed from the close inspection in Fig. 11, the PL intensity peak near 518 nm of ZnO samples increases with the increasing deposition time, which indicates the presence of more surface oxygen vacancies, while increasing the thickness of deposited thin films. This result corroborates with the XPS measurements discussed in the previous section. These surface defects can drastically affect the photocatalytic activity of deposited ZnO thin films.

The intensity of the PL signal is an index that reveals the recombination rate of the photogenerated charge carriers. Lower thicknesses of deposited ZnO thin films exhibit lower PL intensities compared to higher thicknesses, which suggest lower recombination rate of the charge carriers, which can be beneficial for improving its photocatalytic properties.

In addition, and in order to investigate the effect of temperature on the PL emissions, post annealing treatment of the thicker deposited ZnO thin film (720 nm) was performed at 500 °C and 600 °C during 60 minutes. It can be observed that the PL intensity of the deposited thin films increases after annealing treatment (Fig. 11), therefore, it can be concluded that exposing deposited thin films with higher deposition time at elevated temperatures, exhibits the same behavior as performing post-deposition annealing treatment. Moreover, the scattered light from the samples surface (stronger offset) increases due to the change in the surface roughness. A PL shift towards shorter wavelength is also observed (Fig. 11) after post annealing treatment, which can be a result of the scattered light of the excitation beam.

The PL measurements suggest that the photocatalytic activity decreases with increasing spray time and in turn deposited thin films thickness. This can be explained by the increase in the grain size with the spray time, and that thinner thin films have higher surface area (also observed form SEM images). Hence, we get greater interfacial contact with the chemical species in the solution, promoting redox reactions. Also, and as can be observed form the SEM images (Fig 3), the ZnO nano-petals get larger in dimensions, and that the films become denser. Therefore, increasing the spray time leads to grain coalescence, which is shown by the decrease in the water contact angle (Fig 9).

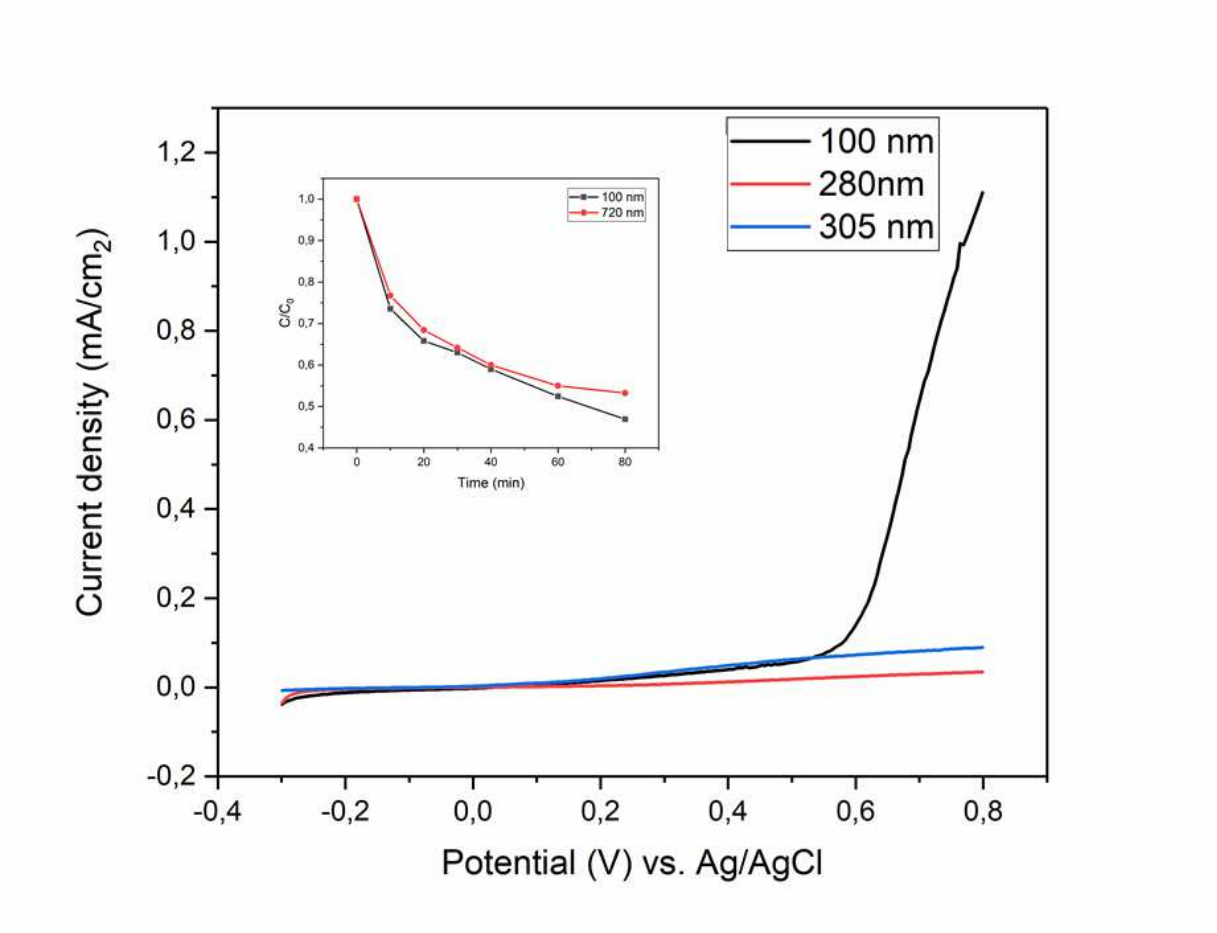

Figure 12. Linear sweep voltammograms of sprayed ZnO thin films with different thicknesses. The insert plot show the MB degradation versus the irradiation time.

The band gap energy was measured from PL spectra, and the results showed that it increases from 3.23 eV to 3.26 eV with increasing the thickness of deposited ZnO thin films. These results are in good agreement with those of theoretical calculations of DFT and calculations from the optical absorption spectra. In order to further confirm these results, the effect of annealing temperature on the bad gap energy was investigated. Deposited ZnO thin films were annealed in the air atmosphere at temperature of 500 °C and 600 °C, during 60min. The band gap energy was calculated from the PL spectra, and the results showed an increasing with the annealing temperature from 3.27 eV at temperature of 500 °C to 3.275 eV at temperature of 600 °C.

The photocatalytic activity of deposited ZnO thin films was assessed by measuring the degradation of methylene blue under UV irradiation. The obtained results show a decrease of

MB degradation rate, with the increase of the film thickness of deposited ZnO thin films (insert Fig. 12).

As shown in Fig. 11, the highest and lowest UV-emission PL peak intensity (381 nm) are observed for deposited ZnO thin film with thicknesses of 305 nm and 100 nm respectively. These results are in good agreement with those of PEC measurement (Fig. 12), which show high photocurrent for deposited ZnO thin film with thickness of 100 nm and its decreases with increasing of thickness. Both the photoluminescence and photo-electrochemical measurements suggest that the photocatalytic activity decreases with increasing the thickness of deposited ZnO thin films.

The photocatalytic reaction is directly related to the grain size of deposited thin films as to the surface area and therefore the recombination rate of the photo-generated electron/hole pairs. The average carrier diffusion time (τ) from the bulk to the surface can be calculated by the following equation:

$$\tau = r^2\pi^2 D \tag{24}$$

Where (r) is the grain's radius, and (D) is the diffusion coefficient of the carrier [59-60]. Therefore, a decrease in the grain radius would reduce the recombination of the photo-generated electron/hole pairs moving to the surface, and therefore improves the photocatalytic performance. Moreover, a decrease in the grain's radius increases the surface area, which leads to the reaction sites increasing.

From the water contact measurements (Fig. 9), a surface wettability transition between hydrophobic and hydrophilic can be observed, which shows that the hydrophilic conversion is favorable with the presence of tensile stress in the films. The effect of internal residual stress on the sprayed ZnO thin films has been shown to increase the photo-induced wetting sensitivity, but not the photocatalytic activity of the films, which is in good agreement with the literature [61].

In summary, from the photoluminescence measurement, which provides information about the charges separation and recombination in the photo-catalysts, it can be observed that the intensity of the PL peak increases with increasing the thickness of deposited ZnO thin films. The higher the intensity of PL signal, the higher the recombination rate of the photo generated

electron/holes, and therefore, the photocatalytic efficiency decreases. This conclusion is supported by the photocatalytic tests conducted on deposited ZnO thin films of different thicknesses, which shows the best MB degradation with ZnO thin film thickness of about 100 nm. Furthermore, PEC measurements provide additional support to this conclusion in terms of higher photocurrent observed with ZnO thin film thickness of about 100 nm, in comparison to thicker films. On the other hand, further support is provided by the bang gap energy increasing with thickness.

4. Conclusion

The ZnO thin films deposited by the spray-ILGAR method were demonstrated to exhibit improved photocatalytic performance with decreasing spray time/film thickness. The XRD data was used to determine the structural parameters such as the crystallite size, lattice parameters, Zn-O bond length, and residual stress, which revealed a decrease in the lattice parameters and a continuous variation in the compressive strain with the increasing spray time and in turn deposited ZnO thin film thickness. Furthermore, it was demonstrated by different techniques that the energy band gap increases as the compressive strain increases, which was confirmed by theoretical first principle calculations using the density functional theory (DFT). These results show that the optical band gap of deposited ZnO thin films can be tuned by the application of compressive strain.

The photocatalytic efficiency is shown to decrease with increasing deposition time, which is explained by the increase in the structural and surface defects with the deposited ZnO thin film thickness. This favor the recombination process of electron/hole pairs.

The wettability of deposited thin films was examined and a wetting behavior switching from hydrophobic to hydrophilic was observed under exposure to UV irradiation. Furthermore, the effect of internal residual stress on the optical properties of sprayed ZnO thin films has been shown to increase the photo-induced wetting sensitivity, but not the photocatalytic activity of deposited thin films.

Funding Acknowledgment

The authors gratefully acknowledge the DAAD (Deutscher Akademischer Austauschdienst) for providing financial support to the first author to conduct this work.

References

[1] D. C. Reynolds, D. C. Look, B. Jogai, C. W. Litton, G. Cantwell and W. C. Harsch, Valence-band ordering in ZnO, Physical Review B 60 (1999) 2340.

[2] V. Srikant, D.R. Clarke, On the optical band gap of zinc oxide, Journal of Applied Physics 83(10) (1998) 5447-5451.

[3] W.J. Li, E.W. Shi, W.Z. Zhong, Z.W. Yin, Growth mechanism and growth habit of oxide crystals, Journal of Crystal Growth 203(1) (1999) 186–196.

[4] E.R. Carraway, A.J. Hoffman, M.R. Hoffmann, Photocatalytic oxidation of organic acids on quantum-sized semiconductor colloids, Environmental Science and Technology 28 (1994) 786-793.

[5] S. Herminghaus, Roughness-induced non-wetting, Europhysics Letters 52(2) (2000) 165-170.

[6] A. Alvarado, J. Attapattu, Y. Zhang, C. Chen, Thermoelectric properties of rocksalt ZnO from first-principles calculations, Journal of Applied Physics 118 (2015) 165101

[7] L. Zhu, W. Zeng, Room-temperature gas sensing of ZnO-based gas sensor: A review, Sensors and Actuators A: Physical 267(1) (2017) 242-261.

[8] B. Hussain, A. Ebong, I. Ferguson, Zinc oxide as an active n-layer and antireflection coating for silicon based heterojunction solar cell, Solar Energy Materials and Solar Cells 139 (2015) 95-100.

[9] S. J. Pearton, F. Ren, Advances in ZnO-based materials for light emitting diodes, Current Opinion in Chemical Engineering 3 (2014) 51-55.

[10] F.D. Nayeri, M. Kolahdouz, E. Asl-Soleimani, S. Mohajerzadeh, Low temperature carving of ZnO nanorods into nanotubes for dye-sensitized solar cell application, J. Alloys Compd. 633 (2015) 359–365.

[11] K. M. Lee, C. W. Lai, K. S. Ngai, J. C. Juan, Recent developments of zinc oxide based photocatalyst in water treatment technology: A review, Water Research 88 (1) (2016) 428-448.

[12] M. Dutta, S. Mridha, D. Basak, Effect of sol concentration on the properties of ZnO thin films prepared by sol–gel technique, Appl. Surf. Sci. 254 (2008) 2743–2747.

[13] M.R. Alfaro Cruz, O. Ceballos-Sanchez, E. Luévano-Hipólito, L.M.Torres-Martínez, ZnO thin films deposited by RF magnetron sputtering: Effects of the annealing and atmosphere conditions on the photocatalytic hydrogen production, International Journal of Hydrogen Energy 43(22) (2018) 10301-10310.

[14] S. Fay, U. Kroll, C. Bucher, E. Vallat-Sauvain, A. Shah, Low pressure chemical vapour deposition of ZnO layers for thin-film solar cells: temperature-induced morphological changes, Sol. Energy Mater. Sol. Cells 86 (2005) 385–397.

[15] C.J. Chang, S.T. Hung, C.K. Lin, C.Y. Chen, E.H. Kuo, Selective growth of ZnO nanorods for gas sensors using ink-jet printing and hydrothermal processes, Thin Solid Films 519 (2010) 1693–1698.

[16] H. Ennaceri, L. Wang, D. Erfurt, W. Riedel, G. Mangalgiri, A. Khaldoun, A. El Kenz, A. Benyoussef, A. Ennaoui, Water-resistant surfaces using zinc oxide structured nanorod arrays with switchable wetting property, Surface and Coating Technology 299 (2016) 169–176.

[17] T. Prasada Rao, M.C. Santhoshkumar, Appl. Surf. Sci. 255 (2009) 4579–4584.

[18] K. Rajeshwar, M. E. Osugi, W. Chanmanee, C. R. Chenthamarakshan, M. V. B. Zanoni, P. Kajitvichyanukul, R. J. Krishnan-Ayer, Heterogeneous photocatalysis treatment of organic dyes in air and aqueous media, Photochemistry and Photobiology C: Photochemistry Reviews 9 (2008) 171-192.

[19] E. Otsuka, K. Kurumada, A. Suzuki, S. Matsuzawa, K. Takeuchi, An application of transparent mesoporous bulk silica to a titanium dioxide photocatalyst with adsorption and decomposition functions, Journal of Sol-Gel Science and Technology 46(1) (2008) 71-78.

[20] I. Sopyan, M. Watanabe, S. Murasawa, K. Hashimoto, A. Fujishima, An efficient TiO2 thin-film photocatalyst: photocatalytic properties in gas-phase acetaldehyde degradation, Journal of Photochemistry and Photobiology Part A: Chemistry 98(1) (1996) 79-86.

[21] W. Y. Gan, M. W. Lee, R. Amal, H. Zhao, K. Chiang, Photoelectrocatalytic activity of mesoporous TiO2 films prepared using the sol-gel method with tri-block copolymer as structure directing agent, Journal of Applied Electrochemistry 38(5) (2008) 703-712.

[22] Y. Wang, Z. Zhang, Y. Zhu, Z. Li, R. Vajtai, L. Ci, P.M. Ajayan, Nanostructured VO2 photocatalysts for hydrogen production, ACS Nano 2(7) (2008) 1492-1496.

[23] J. Yu, H. Yu, B. Cheng, X. Zhao, J. Yu, W. Ho, The effect of calcination temperature on the surface microstructure and photocatalytic activity of TiO2 thin films prepared by liquid phase deposition, Journal of Physical Chemistry B 107(50) (2003) 13871-13879.

[24] V. Khranovskyy, T. Ekblad, R. Yakimova, L. Hultman, Surface morphology effects on the light-controlled wettability of ZnO nanostructures, Applied Surface Science 258 (20) (2012) 8146–8152.

[25] J. Sheng, J. Karasawa, T. Fukami, Thickness dependence of photocatalytic activity of anatase film by magnetron sputtering, J. Mater. Sci. Lett. 16 (1997) 1709–1711.

[26] S. G. Kumar and K. S. R. K. Rao, Zinc oxide based photocatalysis: tailoring surface-bulk structure and related interfacial charge carrier dynamics for better environmental applications, RSC Adv. 2015, 5, 3306–3351.

[27] A. Ramirez-Canon, M. Medina-Llamas, M. Vezzoli, D. Mattia, Multiscale design of ZnO nanostructured photocatalysts, Phys. Chem. Chem. Phys. 2018, 20, 6648-6656.

[28] H. Tada, M. Tanaka, Dependence of TiO2 Photocatalytic Activity upon Its Film Thickness, Langmuir 13 (2) (1997) 360–364.

[29] K. J. Kumar, NRC. Raju, A. Subrahmanyam, Thickness Dependent Physical and Photocatalytic Properties of ITO Thin Films Prepared by Reactive DC Magnetron Sputtering, Applied Surface Science 257(7) (2011) 3075-3080.

[30] P. Dias, A. Vilanova, T. Lopes, L. Andrade, A. Mendes, Extremely stable bare hematite photoanode for solar water splitting, Nano Energy 23 (2016) 70-79.

[31] G. Kenanakis, Z. Giannakoudakis, D. Vernardou, C. Savvakis, N. Katsarakis, Photocatalytic degradation of stearic acid by ZnO thin films and nanostructures deposited by different chemical routes, Catalysis Today 151 (2010) 34-38.

[32] H. Ennaceri, D. Erfurt, L. Wang, T. Köhler, A. Taleb, A. Khaldoun, A. El Kenz, A. Benyoussef, A. Ennaoui, Deposition of multifunctional TiO2 and ZnO top-protective coatings for CSP application, Surface & Coatings Technology 298 (2016) 103–113.

[33] J.M. Myoung, W.H. Yoon, D.H. Lee, I. Yun, S.H. Bae, S.Y. Lee, Effects of Thickness Variation on Properties of ZnO Thin Films Grown by Pulsed Laser Deposition, Japanese Journal of Applied Physics 41 (2002) 28-31.

[34] R. Vinodkumar, K.J. Lethy, P.R. Arunkumar, Renju R. Krishnan, N. Venugopalan Pillai, V.P. Mahadevan Pillai, Reji Philip, Effect of cadmium oxide incorporation on the microstructural and optical properties of pulsed laser deposited nanostructured zinc oxide thin films, Materials Chemistry and Physic 121(3) (2010) 406-413.

[35] B. D. Cullity. Elements of X-Ray Diffraction (2nd ed.) (reading, M A : Addison Wesley) (1978).

[36] P. Scherrer, Bestimmung der Grösse und der inneren Struktur von Kolloidteilchen mittels Röntgenstrahlen,Nachr. Ges. Wiss. Göttingen 26 (1918) 98-100.

[37] B. D. Cullity, S. Rstock, Elements of X-ray Diffraction, Prentice Hall, New Jersey, 2001.

[38] T. P. Rao, M.C. Santhosh kumar, Thickness effect on structural, optical and electrical properties of ZnO thin films by Spray Pyrolysis, Applied Surface Science 255 (2009) 4579-4584.

[39] D. Gedamu, I. Paulowicz, S. Kaps, O. Lupan, S. Wille, G. Haidarschin, Y. K. Mishra, R. Adelung, Rapid Fabrication Technique for Interpenetrated ZnO Nanotetrapod Networks for Fast UV Sensors, Advanced Materials 26 (2014) 1541.

[40] O. Lupan, T. Pauporte, L. Chow, B. Viana, F. Pelle´, L.K. Ono, B. Roldan Cuenya, H. Heinrich, Effects of annealing on properties of ZnO thin films prepared by electrochemical deposition in chloride medium, Applied Surface Science 256 (2010).

[41] H. Morkoç, Ü .Özgür, Zinc Oxide: Fundamentals, Materials and Device Technology. Heidelberg, Germany: Wiley-VCH; 2009.

[42] M.F. Malek, M.H. Mamat, M.Z. Musa, Z. Khusaimi, M.Z. Sahdan, A.B. Suriani, A. Ishak, I. Saurdi, S.A. Rahman, M. Rusop, Thermal annealing-induced formation of ZnO nanoparticles: Minimum strain and stress ameliorate preferred c-axis orientation and crystal-growth properties, Journal of Alloys and Compounds 610 (2014) 575–588.

[43] P.R. Benger, K. Chang, P. Bhattacharya, J. Sing, K.K. Bajaj, Role of strain and growth conditions on the growth front profile of InxGa1−xAs on GaAs during the pseudomorphic growth regime, Appl. Phys. Lett. 53 (1988) 684.

[44] T. Prasada Rao, M. C. Santhosh Kumar, A. Safarulla, V. Ganesan, S. R. Barman, C. Sanjeeviraja, Physical properties of ZnO thin films deposited at various substrate temperatures using spray pyrolysis, Physica B: condensed Matter 405(9) (2010) 2226-2231.

[45] C.S. Barret, F.B. Massalski, Structure of Metals, Pergamon Press, Oxford (1980).

[46] C. Li, X.C. Li, P.X. Yan, E.M. Chong, Y. Liu, G.H. Yue, X.Y. Fan, Research on the properties of ZnO thin films deposited by using filtered cathodic arc plasma technique on glass substrate under different flow rate of O_2, Applied Surface Science 253 (2007) 4000-4005.

[47] J.H. Jou, M.Y. Han, D.J. Cheng, Substrate dependent internal stress in sputtered zinc oxide thin films, Journal of Applied Physics 71 (1992) 4333-4336.

[48] R. Kumar, N. Khare, V. Kumar, G.L. Bhalla, Effect of intrinsic stress on the optical properties of nanostructured ZnO thin films grown by rf magnetron sputtering, Applied Surface Science 254 (2008) 6509-6513.

[49] V. Srikant, D.R. Clarke, Optical absorption edge of ZnO thin films: The effect of substrate, J. Appl. Phys. 81 (1997) 6357.

[50] P. Blaha, K. Schwarz, G. Madsen, D. Kvasnicka, and J. Luitz, WIEN2k, Augmented Plane Wave + Local Orbitals Program for Calculating Crystal Properties, Vienna, Austria, 2001. (See also http://www.wien2k.at)

[51] J. P. Perdew, K. Burke, and M. Ernzerhof, Generalized gradient approximation made simple, Phys. Rev. Lett. 77 (1996) 3865-3868.

[52] F. Tran and P. Blaha, Accurate band gaps of semiconductors and insulators with a semi local exchange-correlation potential. Phys. Rev. Lett. 102 (2009) 226401.

[53] M. Chen, X. Wang, Y. H. Yu, Z. L. Pei, X. D. Bai, C. Sun, R. F. Huang, L. S. Wen, X-ray photoelectron spectroscopy and auger electron spectroscopy studies of Al-doped ZnO films, Appl. Surf. Sci., 158 (2000) 134–140.

[54] J.H. Zheng, Q. Jiang, J.S. Lian, XPS studies and photocurrent applications of alkali-metals-doped ZnO nanoparticles under visible illumination conditions, Appl. Surf. Sci. 257 (2011) 5083-5087.

[55] A. A. Mosquera, D. Horwat, A. Rashkovskiy, A. Kovalev, P. Miska, D. Wainstein, J. M. Albella, J. L. Endrino, Exciton and core-level electron confinement effects in transparent ZnO thin films, Scientific Reports 3 (2015) 1714.

[56] H. Ennaceri, M. Boujnah, A. Taleb, A. Khaldoun, R. Saez-Araoz, A. Ennaoui, A. El Kenz, A. Benyoussef, Thickness effect on the optical properties of TiO2-anatase thin films prepared by ultrasonic spray pyrolysis: Experimental and ab initio study 42(30) (2017) 19467-19480.

[57] X-G. Han, H-Z He, Q. Kuang, X. Zhou, X-H Zhang, T Xu, Z-X. Xie, L-S. Zheng, Controlling Morphologies and Tuning the Related Properties of Nano/Microstructured ZnO Crystallites, J. Phys. Chem. C 113 (2009) 584-589.

[58] N.J. Shirtcliffe, G. McHale, S. Atherton, M.I. Newton, Superhydrophobic textures for microfluidicsAdv. Colloid Interface Sci. 161 (2010) 124-138.

[59] M. Shang, W. Wang, S. Sun, L. Zhou, L. Zhang, Bi2WO6 Nanocrystals with High Photocatalytic Activities under Visible Light, J. Phys. Chem. C 112 (2008) 10407–10411.

[60] A. T. Bell, The Impact of Nanoscience on Heterogeneous Catalysis, Science 299 (2003) 1688-1691.

[61] G. Kenanakis, Z. Giannakoudakis, D. Vernardou, C. Savvakis, N. Katsarakis, Photocatalytic degradation of stearic acid by ZnO thin films and nanostructures deposited by different chemical routes, Catalysis Today 151 (2010) 34-38.